

# No Reference Assessment on Haze for Remote Sensing Images

Xiaoxi Pan, Fengying Xie\*, Zhiguo Jiang, Zhenwei Shi, *Member, IEEE*, and Xiaoyan Luo

## Abstract

**Abstract**—Assessment on haze can filter out images with dense haze to improve the reliability of remote sensing image interpretation. In this paper, a novel no reference haze assessment method based on haze distribution is proposed for remote sensing images. Firstly, range channel of an image is defined and Haze Distribution Map is extracted from the hazy image. Then, the haze assessment metric HDMHA is designed according to the Haze Distribution Map. Finally, the degree of haze in remote sensing images is predicted using the proposed metric. In order to objectively verify the effectiveness of the proposed metric HDMHA, a method of simulating hazy remote sensing images based on haze imaging model is proposed in this paper, and the simulated hazy images are greatly similar with real ones in vision. A series of experiments are done on both real images and simulated images, and the results show that the proposed metric achieves good consistency when compared with subjective experiments and outperforms typical blind image quality assessment methods.

## Index Terms

No reference, Remote sensing images, Haze assessment, Haze distribution map, Haze simulation

## I. INTRODUCTION

Remote sensing images provide a wealth of spatial and geographic information and are widely used for forestry, meteorology, hydrology and military. However, they are easily degraded by atmospheric

This work was supported by the National Natural Science Foundation of China (Grant 61471016 and 61371134).

Xiaoxi Pan, Fengying Xie, Zhiguo Jiang, Zhenwei Shi and Xiaoyan Luo are with the Image Processing Center, School of Astronautics, Beihang University, Beijing, People's Republic of China (e-mail: panxiaoxipamela@163.com, xfy\_73@buaa.edu.cn, jiangzg@buaa.edu.cn, shizhenwei@buaa.edu.cn, luoxy@buaa.edu.cn).

A demo of HDMHA has been made available online: <http://xfy.buaa.edu.cn/>

\*Corresponding author: Fengying Xie.

scattering due to suspended particles in the atmosphere such as haze, fog and mist, which will reduce their application value to a great extent. Therefore, many researchers studied on dehazing to improve image quality. He *et al.* [1] proposed dark channel prior to recover a high-quality haze-free outdoor image. Ancuti *et al.* [2] introduced a fusion-based strategy to single image dehazing, which achieves satisfactory results and can be used for real-time applications. Aliaksei Makarau *et al.* [3] restored the haze-free remote sensing image through subtracting its corresponding haze thickness map which is constructed by searching dark objects locally in the whole image. For some certain applications, remote sensing images from Google Earth are one of the important data sources, such as target detection [4], [5] and classification [6], [7]. This kind of images are also influenced by hazy condition, therefore two fast dehazing methods based on dark channel prior [8] and deformed haze imaging model [9] are proposed respectively to remove haze from Google Earth images. Some researchers also studied on how to evaluate the dehazing effects. Fang *et al.* [10] proposed an evaluation metric combining the ascension of contrast degree with the structural similarity to assess the image quality after dehazing.

Although these dehazing methods mentioned above can improve the quality of hazy images, few studies address the problem of objective assessment on haze in the current literatures. Actually, it is highly necessary for remote sensing image application to develop a metric to evaluate the degree of haze. It can not only help to reduce over or under dehazing phenomena for haze removal algorithms, but also filter out the image with dense haze to improve the reliability of subsequent image analysis.

No reference image quality assessment (IQA) methods are needed for hazy remote sensing images since their reference image is not available. Generally, no reference IQA methods can be classified into two categories [11]: 1) algorithms developed for specific types of distortion, such as blur [12], JPEG and JPEG2000 compression [13], [14], noise [15]; 2) non-distortion-specific algorithms. Moorthy *et al.* [16] proposed a two-step framework (BIQI) for no reference image quality assessment based on natural scene statistics, which did not require any prior knowledge of the distorting process once trained. Tang *et al.* [17] developed a learning based blind image quality measure (LBIQ) which learns a mapping from features of an image to the corresponding subjective quality score to predict the visual quality of images. However, haze is different from distortions mentioned above and the current IQA methods cannot be used for assessing the hazy image quality directly. In this paper, a novel haze assessment algorithm is proposed for Google Earth images. The Haze Distribution Map (HDM) is first extracted from the hazy image and the metric to evaluate the degree of haze in the image is then calculated according to haze distribution.

The structure of the remaining paper is as follows. Section II describes the novel assessment algorithm in

detail. In section III, a haze simulation method is proposed to evaluate the haze degree metric objectively, and section IV analyzes and discusses experimental results for the proposed algorithm. Lastly, conclusion is given in section V.

## II. ASSESSMENT ON HAZE

### A. Haze Distribution Map

We define range channel of an image as the maximum gap value between its three channels, which is computed through:

$$\mathbf{I}^{\text{range}}(\mathbf{x}) = \max_{c \in (r,g,b)} \mathbf{I}^c(\mathbf{x}) - \min_{c \in (r,g,b)} \mathbf{I}^c(\mathbf{x}) \quad (1)$$

where  $\mathbf{x} = (x, y)$  represents the coordinate of a pixel,  $\mathbf{I}$  is the observed intensity and  $\mathbf{I}^c$  stands for a color channel of  $\mathbf{I}$ .

Since the haze is always gray visually, the values of a hazy pixel in R, G, B channels should be equal or close. It means that values of the range channel in hazy regions are small. We manually pick out 5000 hazy patches with size 50x50 pixels from Google Earth, and their range channels are calculated through (1). Fig. 1(a) is the intensity histogram over all 5000 range channels of hazy patches and Fig. 1(b) is the corresponding cumulative distribution. It can be seen that the intensity of about 99 percent of the pixels in the range channel is below 10. That means the three values in R, G, B channels are close enough for a hazy patch in the image.

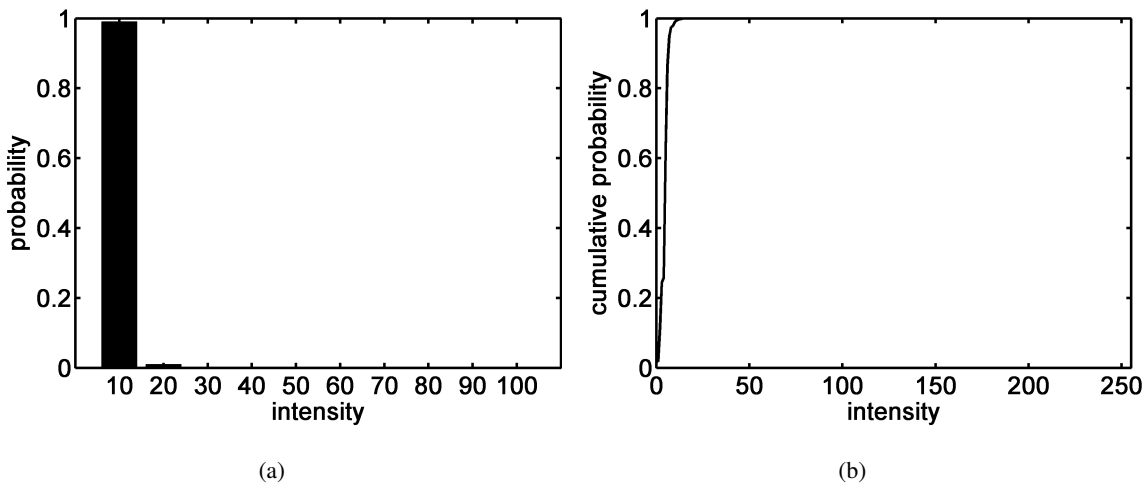


Fig. 1. Statistical results. (a) Histogram of the intensity of range channels for 5000 patches. (b) Cumulative distribution.

According to the dark channel prior [1], for the haze-free patch, at least one color channel has some pixels whose intensities are very low and even close to zero. Moreover, for the hazy patch, the maximum

and minimum among R, G, B channels proved close through the analysis above. Those imply that the minimum intensity in hazy region is higher than that in haze-free region. Therefore, the minimum value among R, G, B channels can reflect the haze distribution in the image roughly. First, the hazy image  $\mathbf{I}$  is normalized to  $[0, 1]$ , denoted as  $\mathbf{I}_N$ . Thus, we define Haze Distribution Map (HDM) as:

$$\mathbf{H}(\mathbf{x}) = \min_{c \in (r, g, b)} \mathbf{I}_N^c(\mathbf{x}) \quad (2)$$

The raw Haze Distribution Map (HDM) can be obtained by (2). Figs. 2 (a) and (b) show a generation instance of HDM for a hazy remote sensing image. As can be seen, on the Haze Distribution Map, the intensity of dense haze region is higher than that of the haze-free region.

Ideally, the intensity of haze-free region in the HDM is expected to be close to zero according to dark channel prior. However, it is not in fact [9] (see the red circle in Fig. 2(b)). Therefore the raw HDM needs to be corrected. It is known that saturation represents the purity of color, and for an image, the larger its saturation, the more vivid its color. Fig. 2(c) is the saturation of Fig. 2(a). Obviously, the saturation in haze-free region is higher than that in hazy region. Thus, for the haze-free region, the intensity of its HDM is low, on the contrary, the corresponding saturation is high. In order to decrease the intensity of haze-free region and obtain a more precise HDM, the saturation  $\mathbf{S}(\mathbf{x})$  is subtracted from (2):

$$\tilde{\mathbf{H}}_s(\mathbf{x}) = \max(\mathbf{H}(\mathbf{x}) - \alpha \mathbf{S}(\mathbf{x}), 0) \quad (3)$$

$$\mathbf{S}(\mathbf{x}) = 1 - \frac{3\min(\mathbf{R}(\mathbf{x}), \mathbf{G}(\mathbf{x}), \mathbf{B}(\mathbf{x}))}{\mathbf{R}(\mathbf{x}) + \mathbf{G}(\mathbf{x}) + \mathbf{B}(\mathbf{x})} \quad (4)$$

where  $\mathbf{R}, \mathbf{G}, \mathbf{B}$  represent three color channels,  $\alpha$  is an adjusting parameter to make the haze-free region dark enough and it is fixed to 2 in the paper. The  $\max$  operator in (3) is used to avoid negative values. Fig. 2(d) shows the corrected HDM obtained through (3). It can be seen that the intensity of haze-free region (red circle) in Fig. 2(d) is lower than that in Fig. 2(b). At the same time, in order to weaken the impact of scene texture on HDM, morphological opening operation and a guided filter [18] are carried out on the corrected HDM as post processing. Fig. 2(e) is the final HDM after post processing, which is denoted as  $\mathbf{H}_s$ .

### B. Haze Assessment

In vision systems, the influence of haze on images depends on haze density and its coverage area. When the haze is dense and covers a large area, its influence on image quality is serious. For the haze-free remote sensing image, the intensity of its HDM is low. The denser the haze becomes, the higher the intensity will be. Therefore, we propose a metric named HDM-based Haze Assessment (HDMHA)

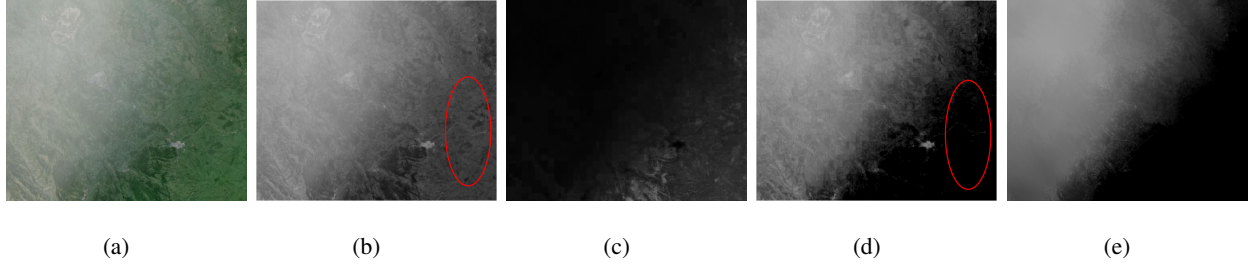


Fig. 2. Haze Distribution Map of a hazy image. (a) Hazy image. (b) Raw HDM. (c) Saturation map. (d) Corrected HDM. (e) HDM

to predict the degree of haze for remote sensing images visually. First, the HDM is divided into  $n$  nonoverlapping small patches. When the patch size is small enough, each patch can be assumed to be either clear or hazy. Then the assessment metric of haze for  $i$ th patch can be computed through:

$$\text{HDMHA}_i = \frac{2 \min_{y \in \Omega(x)} \mathbf{H}_s(\mathbf{y})}{\max(T, \max_{y \in \Omega(x)} \mathbf{H}_s(\mathbf{y})) + \min_{y \in \Omega(x)} \mathbf{H}_s(\mathbf{y})} \quad (5)$$

where  $\Omega(\mathbf{x})$  is a local patch centered at  $\mathbf{x}$ ,  $T$  ( $0.5 \leq T \leq 1$ ) is a parameter which should be a large value to keep the denominator at a high level for both clear and hazy patches. When  $T$  is small, its effect will be reduced and the metric value of a slightly hazy patch becomes large, which weakens the separability between slightly hazy patches and densely hazy patches. On the other hand, if the value of  $T$  is too large, the range of the metric value will be narrowed, consequently, the metric cannot reflect human's subject perception very well. Here,  $T$  is fixed to 0.8 in this paper. The blind assessment property of the proposed metric can be explained intuitively as follows.

Case 1: "haze-free patch." The intensity of the HDM is very low and the minimum  $\ll 0.8$ , so  $\text{HDMHA} \approx 0$ .

Case 2: "hazy patch." The intensity of the HDM is very high and maximum  $\approx$  minimum, so  $\text{HDMHA} \approx 1$ .

The HDMHA metric is developed under the assumption that the patch is binary: clear or hazy, which requires the patch is small enough. Obviously, it will be computationally burdensome when pursuing an accurate evaluation result. However, on the other hand, a large patch size will lead to an inaccurate prediction, for example, two patches shown in Fig. 3. Clearly, patch A is influenced more seriously by haze than patch B. However, the real quantitative assessment result is  $\text{HDMHA}_A = \text{HDMHA}_B$  ( $\min_A = \min_B = 0$ ,  $\max_A = \max_B = 0.9502$ ) because the metric  $\text{HDMHA}_i$  depends on the minimal value in a patch. In order to balance the accuracy and time cost, the minimum operator in the numerator

of (5) is replaced by mean operator and the assessment index for  $i$ th patch is redefined as:

$$\text{HDMHA}_i = \frac{2\text{mean}_{y \in \Omega(x)} \mathbf{H}_s(\mathbf{y})}{\max(T, \max_{y \in \Omega(x)} \mathbf{H}_s(\mathbf{y})) + \min_{y \in \Omega(x)} \mathbf{H}_s(\mathbf{y})} \quad (6)$$

Through (6),  $\text{HDMHA}_A$  is larger than  $\text{HDMHA}_B$ , which is in an agreement with the reality.

For the whole image, our proposed metric is expressed as:

$$\text{HDMHA} = \frac{1}{n} \sum_{i=1}^n \text{HDMHA}_i \quad (7)$$

Therefore, a large HDMHA value indicates dense and widespread haze in a remote sensing image.

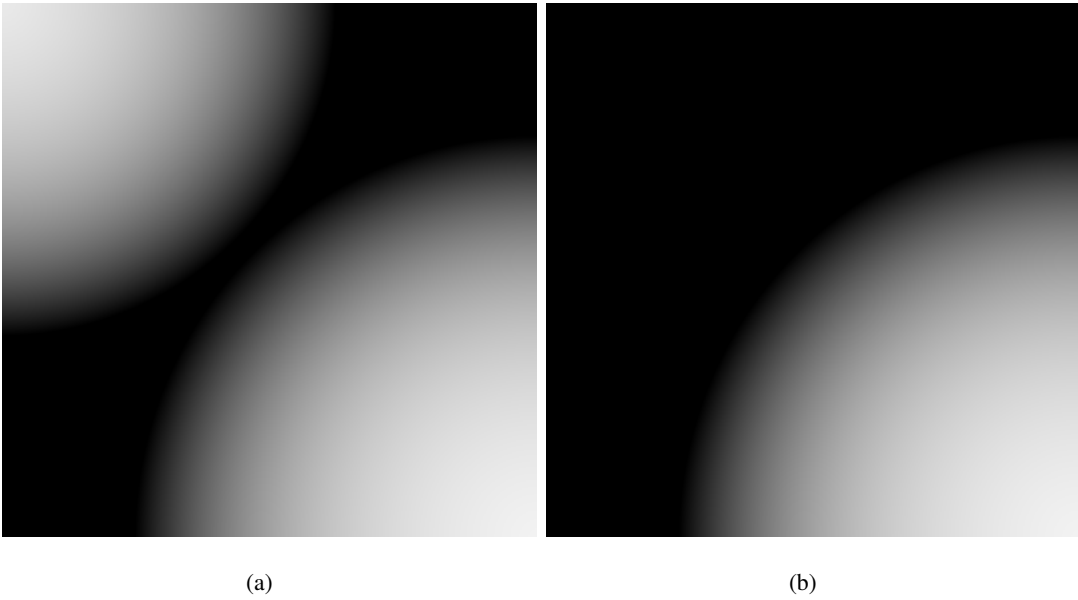


Fig. 3. Simulated HDMs of hazy patches. (a) Patch A. (b) Patch B.

### III. SIMULATION OF HAZY REMOTE SENSING IMAGES

Since few studies about haze assessment can be found, the publicly available IQA datasets such as LIVE II [19], TID [20] and CSIQ [21] do not contain hazy remote sensing images. In this section, a simulation method for hazy images is proposed.

#### A. Transmission Extraction

According to [22], [23], the haze imaging model can be described on the RGB color channels as:

$$\mathbf{I}(\mathbf{x}) = \mathbf{J}(\mathbf{x})\mathbf{t}(\mathbf{x}) + \mathbf{A}(1 - \mathbf{t}(\mathbf{x})) \quad (8)$$

where  $\mathbf{J}(\mathbf{x})$  stands for the scene radiance,  $\mathbf{t}(\mathbf{x})$  is the transmission and  $\mathbf{A}$  is the atmospheric light. Transmission  $\mathbf{t}(\mathbf{x})$  cannot be obtained directly by (8) because  $\mathbf{J}(\mathbf{x})$  is unknown. Through the derivation in [1], the transmission can be estimated as:

$$\tilde{\mathbf{t}}(\mathbf{x}) = 1 - \min_{\mathbf{y} \in \Omega(\mathbf{x})} \left( \min_{c \in (r, g, b)} \frac{\mathbf{I}^c(\mathbf{y})}{\mathbf{A}^c} \right) \quad (9)$$

Obviously,  $\tilde{\mathbf{t}}(\mathbf{x})$  is image-derived [8] and it can be obtained through computing.

Then a guided filter [18] is used to avoid block artifacts in the raw transmission extracted by (9). Generally, the grayscale image of  $\mathbf{I}$  is used as the guidance image but the texture cannot be avoided. In this paper, a black image is adopted as the guidance image to overcome the original scene texture. Fig. 4 shows remote sensing images and their corresponding transmissions.

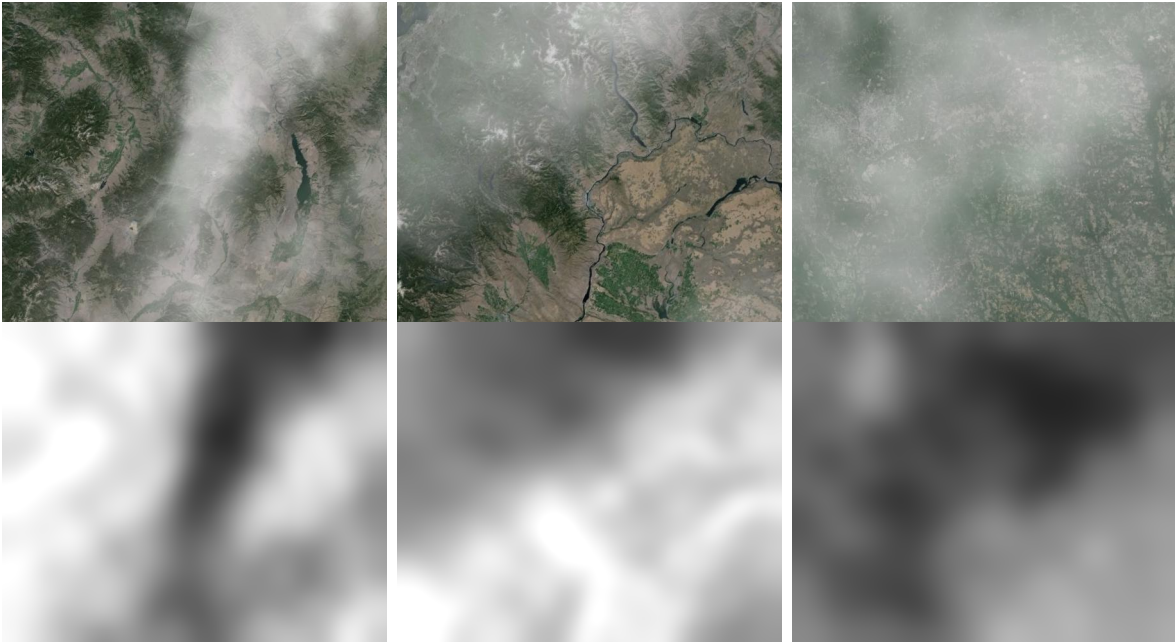


Fig. 4. Instances of extracted transmissions, where the first row shows hazy images and the second row shows their corresponding transmissions.

### B. Hazy Remote Sensing Images Simulation

We take the transmissions extracted from real hazy images as haze masks, and add them to clear images through the haze imaging model (8) to simulate hazy images. According to (8), once the scene radiance  $\mathbf{J}(\mathbf{x})$  (clear image), transmission  $\mathbf{t}(\mathbf{x})$  and atmospheric light  $\mathbf{A}$  are given, the hazy image can be generated. For a fixed atmospheric light  $\mathbf{A}$ , images with different haze distribution can be obtained

through using different transmissions  $t(\mathbf{x})$  extracted from real hazy images. As shown in Fig. 5, where (a) is the reference image, (b) and (c) are two images with different haze distributions generated by the first two transmissions in Fig. 4. Similarly, for a fixed transmission  $t(\mathbf{x})$ , images with different haze densities can be obtained through adjusting the value of atmospheric light  $\mathbf{A}$ . As shown in Fig. 6, these images are synthesized using the same scene and same transmission under different atmospheric light, where the transmission is from the last one in Fig. 4. Furthermore, hazy images under different scenes can be generated as well, which is shown in Fig. 7. From Fig. 5 to Fig. 7, it can be seen that these synthetic images are highly close to real hazy images in vision, which is in favor of the validation for the algorithm's performance.

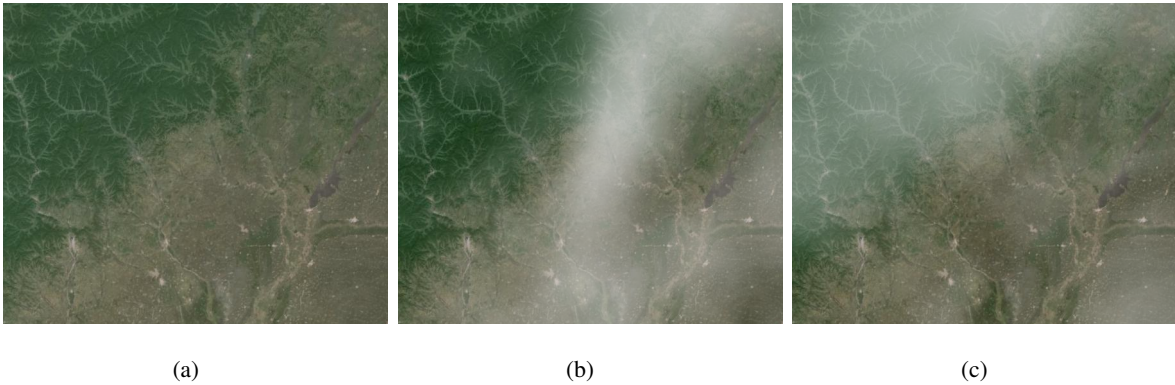


Fig. 5. Hazy images simulated using **different** transmissions. (a) Reference image. (b) and (c) are synthetic images.

#### IV. EXPERIMENTAL RESULTS

In order to analyze the performance of our method, a series of experiments are done on the PC with 3.1GHz Intel Core i5 Processor using Matlab 2013a.

We have two datasets: simulated dataset and real dataset. In our simulated dataset, 80 transmissions are extracted from 80 real hazy remote sensing images and each of them can be used to generate 4 levels of haze (Level 2–Level 5 shown in Fig. 6). For 20 clear reference images, totally 6400 hazy remote sensing images are obtained. In real dataset, 65 real hazy remote sensing images are used for subjective experiment, which are different from the 80 hazy images used for generating the simulation dataset. All the real images (145 (65 + 80) hazy images and 20 haze-free images) are from Google Earth and they are with the size of  $500 \times 600$  pixels, and the metric HDMHA is computed using a patch size of  $20 \times 20$  pixels.

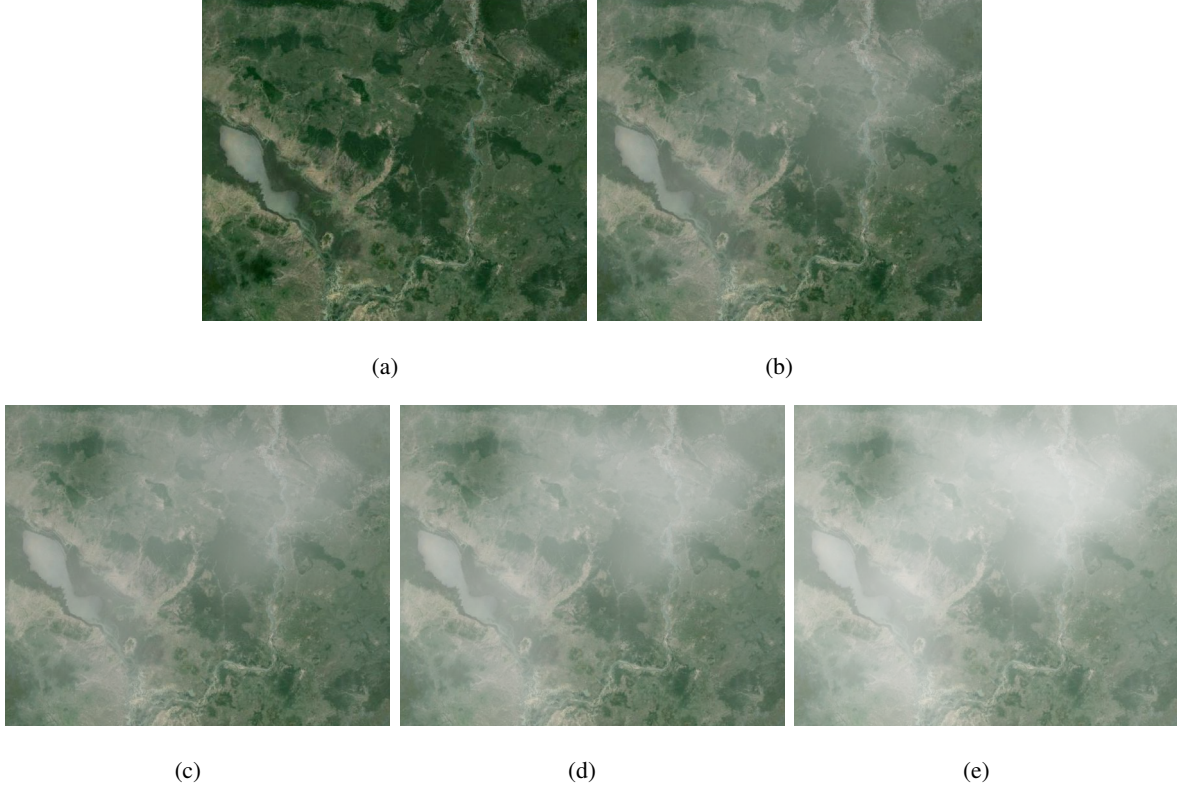


Fig. 6. Hazy images simulated using the **same** transmission and **same** scene. (a) Reference image (Level 1) (b) Level 2 (c) Level 3 (d) Level 4 (e) Level 5

#### A. Assessment on Simulated Hazy Remote Sensing Images

To test the effectiveness of the proposed metric objectively, experiments are carried out from two aspects: haze assessment under different densities and under different distributions. In the existing IQA methods, haze assessment is barely mentioned. Two state-of-art no reference IQA methods BIQI [16] and NIQE [24], which are non-distortion-specific, and the full reference index SSIM [25] are compared with our algorithm.

1) *Experiments for simulated images with different densities of haze:* We divide 6400 simulated hazy images into 80 groups in terms of different transmissions. In each group, for the same reference image, there are 4 levels (Level 2–Level 5) of haze. Considering additional 20 reference images, there are totally 100 images (80 simulated hazy images and 20 reference images) in a group. For images in each group, we first extract their HDMs using the method described in section II-A, and then calculate the metric HDMHA through (6) and (7). Fig. 8 shows the distribution of HDMHA values of random two groups. Clearly, for different level of haze, the values of metric HDMHA are separated very well, which means

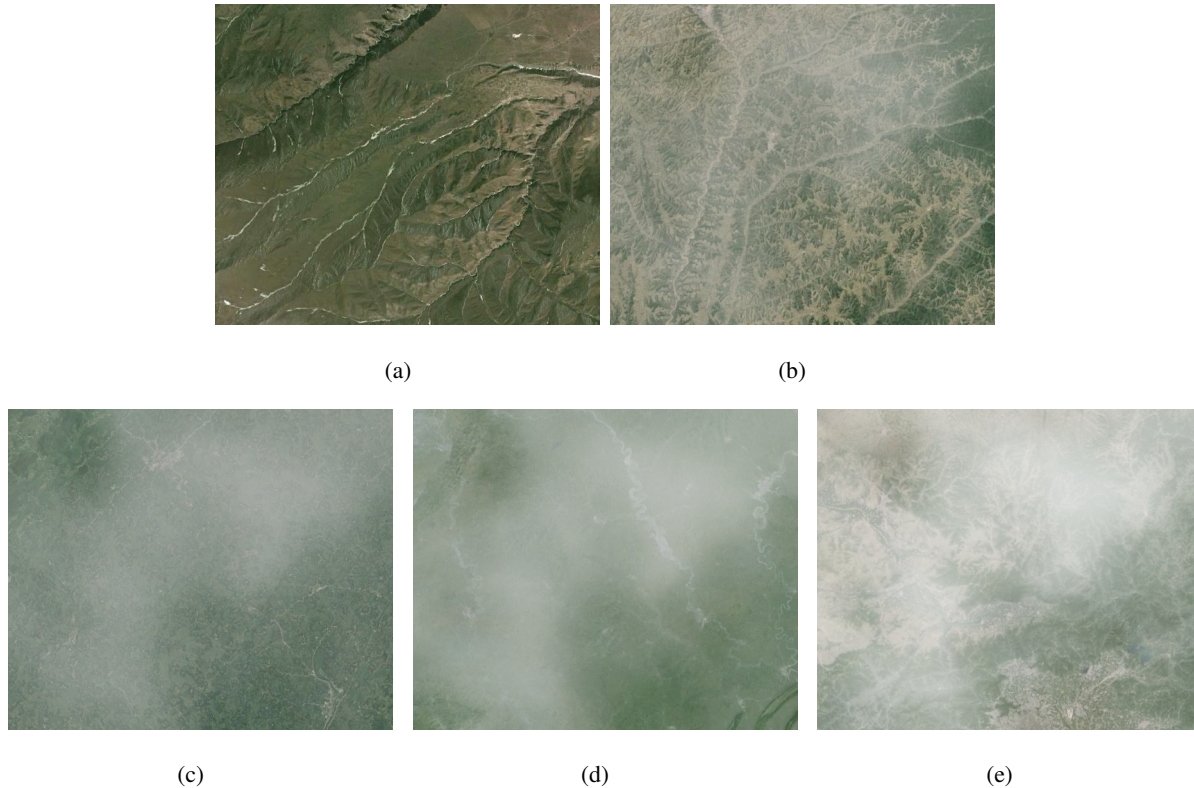


Fig. 7. Hazy images simulated using the **same** transmission but **different** scenes. (a) Reference image (Level 1) (b) Level 2 (c) Level 3 (d) Level 4 (e) Level 5

that HDMHA can reflect the variation of haze density correctly.

Fig. 6 and Fig. 7 are simulated hazy remote sensing images using the same transmission under different scenes, in which (a) to (e) denote 5 levels of haze degree respectively. Their HDMHA values are shown in Table I. It can be seen that the metric HDMHA becomes larger as the haze density increases, which coincides with the visual observation. Theoretically, HDMHA values for hazy images in Fig. 6 and Fig. 7 should be equal since they are simulated using the same transmission and atmospheric light. The slight errors between Fig. 6 and Fig. 7 are attributed to different scenes. The maximum variance in dataset caused by different scenes is 0.0744 and it demonstrates that the proposed metric HDMHA is insensitive to the scene.

We then use two important evaluation criteria: Pearson linear correlation coefficient (LCC) and Spearman rank-order correlation coefficient (SROCC) to analyze the performance of IQA methods and higher values indicate better performances. The simulated haze level is used as the ground truth and the evaluation results for the four metrics on all the 80 groups are given in Table II. As can be seen, the proposed

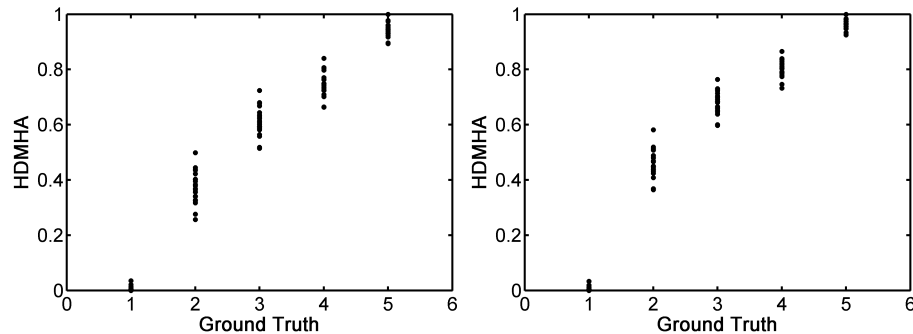


Fig. 8. Assessment on different haze densities using HDMHA

TABLE I  
ASSESSMENT RESULTS FOR SIMULATED IMAGES USING HDMHA

HDMHA	(a)	(b)	(c)	(d)	(e)
Fig. 6	0.0095	0.3723	0.5733	0.6894	0.8384
Fig. 7	0	0.4220	0.6387	0.7127	0.8569

metric HDMHA performs better than both BIQI and NIQE, and meanwhile, it is comparable to the full reference index SSIM.

TABLE II  
MEAN CORRELATION COEFFICIENT OF 80 GROUPS

	BIQI	NIQE	SSIM	HDMHA
LCC	0.3917	0.4744	0.9536	0.9445
SROCC	0.4024	0.4020	0.9603	0.9785

2) *Experiment for simulated images with different distributions of haze:* In this experiment, we choose 1600 hazy images with level 4 from the simulated dataset as experimental images (80 transmissions  $\times$  20 reference images). They are then divided into 20 groups in terms of different reference images and each group consists of 80 hazy images. Here, the theoretical ground truth is unavailable. Considering the full-reference SSIM index represents the similarity between a reference image and its corresponding distorted image, and it is positive correlation with image quality. Therefore, in this paper, the value of 1-SSIM is viewed as the ground truth and a higher value indicates denser haze. The statistical results of LCC and

SROCC for the three no reference metrics are presented in Table III. It can be seen that our proposed metric is still superior to the other two state-of-art approaches.

TABLE III  
MEAN CORRELATION COEFFICIENT OF 20 GROUPS

	BIQI	NIQE	HDMHA
LCC	0.5650	0.2486	0.9588
SROCC	0.5258	0.2295	0.9905

### B. Assessment on Real Hazy Remote Sensing Images

Here, the real dataset is used for the subjective experiment. For some real hazy remote sensing images shown in Fig. 9, the HDMHA values are 0.1504, 0.1648, 0.4509, 0.9565, respectively, which is in reasonable agreement with the human perception. For the whole dataset, we take Mean opinion score (MOS) values computed from subjective scores as the ground truth and a higher value represents denser haze in the image. The correlation indices between MOS and the three no reference metrics are tabulated in Table IV respectively. Clearly, the blind assessment index HDMHA has a higher correlativity with the subjective assessment than BIQI and NIQE.



Fig. 9. Real hazy remote sensing images

TABLE IV  
CORRELATION COEFFICIENT OF REAL HAZY IMAGES

	BIQI	NIQE	HDMHA
LCC	0.1703	0.1117	0.8982
SROCC	0.1122	0.0999	0.9272

## V. CONCLUSION

The application of remote sensing images is affected by haze condition. Assessment for haze can ensure that remote sensing images getting into interpretation system are with high quality, which improves the reliability of automatic interpretation. A method is proposed to evaluate the degree of haze for remote sensing images in this paper. Firstly, Haze Distribution Map is defined as the minimum value in RGB color channels according to dark channel prior and the proposed range channel. Then, on the basis of the HDM, the index HDMHA reflecting the haze density and coverage area is developed. In order to objectively evaluate the performance of the proposed metric, a haze simulation method based on haze imaging model is designed, by which generated hazy remote sensing images are highly close to real hazy images. Experiments are done on both simulated and real remote sensing images and results demonstrate that the proposed method has a strong correlation with the ground truth.

## REFERENCES

- [1] K. He, J. Sun, and X. Tang. "Single image haze removal using dark channel prior," *IEEE Trans. Pattern Anal. Mach. Intell.*, vol. 33, no. 12, pp. 2341-2353, Dec. 2011.
- [2] C. O. Ancuti and C. Ancuti. "Single image dehazing by multi-scale fusion," *IEEE Trans. Image Process.*, vol. 22, no. 8, pp. 3271-3282, Aug. 2013.
- [3] A. Makarau, R. Richter, R. Muller R, and P. Reinartz. "Haze detection and removal in remotely sensed multispectral imagery," *IEEE Trans. Geosci. Remote Sensing*, vol. 52, no. 9, pp. 5895-5905, 2014.
- [4] Z. An and Z. Shi. "Scene learning for cloud detection on remote-sensing images," *IEEE J. Selected Topics in Applied Earth Observations and Remote Sensing*, vol. 8, no. 8, pp. 4206-4222, 2015.
- [5] Z. Shi, X. Yu, Z. Jiang, *et al.* "Ship detection in high-resolution optical imagery based on anomaly detector and local shape feature," *IEEE Trans. Geosci. Remote Sensing*, vol. 52, no. 8, pp. 4511-4523, 2014.
- [6] Dikmen M and Halici U. "A Learning-Based Resegmentation Method for Extraction of Buildings in Satellite Images," *IEEE. Geosci. Remote Sens. Letters*, vol. 11, no. 12, pp. 2150-2153, 2014.
- [7] Aksoy S, Yalniz I Z, Tasdemir K. "Automatic Detection And Segmentation Of Orchards Using Very High Resolution Imagery," *IEEE Trans. Geosci. Remote Sensing*, vol. 50, no. 8, pp. 3117-3131, 2012.
- [8] J. Long, Z. Shi, W. Tang, and C. Zhang. "Single remote sensing image dehazing," *IEEE. Geosci. Remote Sens. Letters*, vol. 11, no. 1, pp. 59-63, Jan. 2014.
- [9] X. Pan, F. Xie, Z. Jiang, and J. Yin. "Haze removal for a single remote sensing image based on deformed haze imaging model," *IEEE Signal Process. Lett.*, vol. 22, no. 10, pp. 1806-1810, 2015.
- [10] S. Fang, J. Yang, J. Zhan J, *et al.* "Image quality assessment on image haze removal," in *Proc. IEEE Control and Decision Conference (CCDC)*, pp. 610-614, 2011.
- [11] Y. Lu, F. Xie, Y. Wu, *et al.* "No reference uneven illumination assessment for dermoscopy images," *IEEE Signal Process. Lett.*, vol. 22, no. 5, pp. 534-538, 2015.
- [12] Z. Cao, Z. Wei, G. Zhang. "A no-reference sharpness metric based on the notion of relative blur for Gaussian blurred image," *J. Vis. Commun. Image R.*, vol. 25, no. 7, pp. 1763-1773, 2014.

- [13] S. Corchs, F. Gasparini, R. Schettini. "No reference image quality classification for JPEG-distorted images," *Digit. Signal Process.*, vol. 30, pp. 86-100, 2014.
- [14] L. Liang, S. Wang, J. Chen, *et al.* "No-reference perceptual image quality metric using gradient profiles for JPEG2000," *Signal Processing: Image Communication*, vol. 25, no. 7, pp. 502-516, 2010.
- [15] M. Liu, G. Zhai, Z. Zhang Z, *et al.* "Blind image quality assessment for noise," in *Proc. IEEE Int. Symposium BMSB*, pp. 1-5, 2014.
- [16] A. K. Moorthy and A. C. Bovik. "A two-step framework for constructing blind image quality indices," *IEEE Signal Process. Lett.*, vol. 17, no. 5, pp. 513-516, 2010.
- [17] H. Tang, N. Joshi and A. Kapoor. "Learning a blind measure of perceptual image quality," in *Proc. CVPR*, 2011, 305-312.
- [18] K. He, J. Sun, and X. Tang. "Guided image filtering," *IEEE Trans. Pattern Anal. Mach. Intell.*, vol. 35, no. 6, pp. 1397-1409, Jun. 2013.
- [19] H. R. Sheikh, Z. Wang, L. Cormack, and A. C. Bovik. Live image quality assessment database release 2. <http://live.ece.utexas.edu/research/quality/subjective.htm>.
- [20] N. Ponomarenko, V. Lukin, A. Zelensky, *et al.* "TID2008-a database for evaluation of full-reference visual quality assessment metrics," *Advances of Modern Radioelectronics*, vol. 10, no. 4, pp. 30-45, 2009.
- [21] E. Larson and D. Chandler. Categorical image quality (csiq) database 2009. <http://vision.okstate.edu/csiq>.
- [22] S. G. Narasimhan and S. K. Nayar. "Vision and the atmosphere," *Int. J. Comput. Vision*, vol. 48, no. 3, pp. 233-254, 2002.
- [23] S. G. Narasimhan and S. K. Nayar. "Chromatic framework for vision in bad weather," in *Proc. CVPR*, 2000, vol. 1, pp. 598-605.
- [24] A. Mittal, R. Soundararajan and A. C. Bovik. "Making a completely blind image quality analyzer," *IEEE Signal Process. Lett.*, vol. 20, no. 3, pp. 209-212, 2013.
- [25] Z. Wang, A. C. Bovik, H. R. Sheikh and E. P. Simoncelli. "Image quality assessment: from error visibility to structural similarity," *IEEE Trans. Image Process.*, vol. 13, no. 4, pp. 600-612, 2004.